PCCP

PAPER

View Article Online
View Journal | View Issue

Cite this: *Phys. Chem. Chem. Phys.*, 2015, **17**, 10953

Laboratory study on OH-initiated degradation kinetics of dehydroabietic acid†

Chengyue Lai, Yongchun Liu,* Jinzhu Ma, Qingxin Ma and Hong He*

Received 16th January 2015,
Accepted 14th March 2015

DOI: 10.1039/c5cp00268k

www.rsc.org/pccp

Dehydroabietic acid (DHAA) is a specific organic tracer for the pyrolysis of conifer resin. To understand its atmospheric stability, the degradation behavior of particulate DHAA in the presence of hydroxyl radicals (OH) was investigated under different environmental conditions using a stainless steel reactor with volume of 30 cm^3, in the dark. At 25 °C and 40% relative humidity (RH), the second-order rate constant (k_2) of pure DHAA with OH was measured to be $5.72 \pm 0.87 \times 10^{-12}$ cm^3 $molecule^{-1}$ s^{-1}. The influence of temperature, RH and mixing state on the degradation kinetics of DHAA were also investigated. At 40% RH, k_2 of pure DHAA increases with increasing temperature and follows the Arrhenius equation $k_2 = (8.9 \pm 1.9) \times 10^{-10} \exp[-(1508.2 \pm 64.2)/T]$, while RH does not have significant impact on k_2 at 25 °C. At 25 °C and 40% RH, compared with pure DHAA, the corresponding k_2 for DHAA mixed with $(NH_4)_2SO_4$ decreased to $4.58 \pm 0.95 \times 10^{-12}$ cm^3 $molecule^{-1}$ s^{-1}, while the value was $3.30 \pm 0.79 \times 10^{-12}$ cm^3 $molecule^{-1}$ s^{-1} when mixed with soot. The atmospheric lifetime of DHAA varied from 2.3 ± 0.2 to 4.4 ± 0.8 days under different environmental conditions. This study indicates that degradation of DHAA by OH radicals is appreciable, and a significant error in source apportionment should be introduced if the contribution of degradation to DHAA concentration is not considered during air mass aging.

Introduction

Organic aerosols contain significant fractions of fine particles, and hundreds of thousands of individual organic species derived from biogenic, anthropogenic and photochemical sources.[1,2] These aerosols affect the radiation budget of Earth, and can cause adverse health effects on humans.[3] Therefore, to protect both human health and the environment, it is important to control the emissions at the source and implement effective reduction measurements on local, regional and global scales.[4,5] Comprehensive investigations are required to evaluate which sources contribute to the total mass of organic aerosols.[6,7] Source apportionment techniques, such as chemical mass balance (CMB) and positive matrix factorization (PMF) receptor models, have been developed and used successfully for quantitative identification of sources for organic pollutants in aerosols.[8–13] In both CMB and PMF models, concentrations of tracers to $PM_{2.5}$ and total organic carbon for different sources are crucial as input parameters. Organic tracers are becoming more commonly used as source indicators because they are specific to the sources of pollutants.[14]

Biomass burning is one of the main sources of fine primary carbonaceous aerosols in the form of organic carbon (OC) and black carbon (BC) on the global scale.[15] The emissions from biomass burning are estimated to contribute up to 38% of tropospheric O_3, 39% of particulate organic carbon and more than 86% of elemental carbon.[16–18] Biopolymers such as cellulose, lignin, hemicellulose, suberlin, sporopollenin, chitin, *etc.* are the major constituents of the biomass.[19] Dehydroabietic acid (DHAA, chemical structure shown in Fig. 1) is a main component of particles emitted through biomass burning. It is the major marker compound emitted from conifer fuel combustion, and can be used to distinguish softwood from hardwood combustion.[19–22] As coniferous tree species represent an important fraction of regional forest composition, DHAA can be emitted from both residential heating and wildfires.[23,24] The detritus of conifer wood burning smoke can also be oxidized

State Key Joint Laboratory of Environment Simulation and Pollution Control, Research Center for Eco-Environmental Sciences, Chinese Academy of Sciences, Beijing, 100085, China. E-mail: ycliu@rcees.ac.cn, honghe@rcees.ac.cn

† Electronic supplementary information (ESI) available: Including detailed experimental procedures for OH determination, preparation procedures for the mixed samples, discussions about the diffusion corrections, a table about the size of mixed samples and figures about the set-up and the mixed sample images. See DOI: 10.1039/c5cp00268k

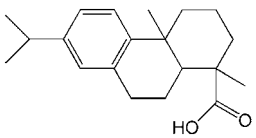

Fig. 1 Chemical structure of dehydroabietic acid (DHAA).

to DHAA, making it the key tracer for the air mass affected by conifer burning.[25] In addition to the natural sources, some anthropogenic sources can also emit DHAA, such as the pulp and paper industry, as well as production of commercial disproportionated rosin. DHAA can be detected easily in the atmosphere,[17,26–28] and some studies have found similar concentration levels of DHAA in the atmosphere compared with another organic tracer, levoglucosan.[5] Because of its ubiquity in the atmosphere and specificity for conifer combustion, DHAA has recently been used as a molecular tracer in source apportionment.[25,29–35] DHAA also represents a series of compounds which make up high proportions of organic aerosols in the atmosphere.

A basic assumption in source apportionment models is that the tracers should have sufficient stability to persist in the atmosphere. In previous studies, particle-phase biomass burning tracers were all thought to be sufficiently stable,[35] but a few recent studies have indicated that some tracers have high reactivity to oxidizing radicals, based on chamber experiments, field observations[1,32,36–43] and quantum chemical calculations.[44–46] As for DHAA, there are only limited studies which have investigated its photolysis degradation in water[47] and biodegradation in the environment by microorganisms.[48] Leithead *et al.* also pointed out that DHAA may be unstable in the atmosphere.[31] Using quantum chemical methods, Bai *et al.* investigated the reaction mechanism and rate constants for DHAA–OH and DHAA–O_3 reactions in the gas phase.[49] However, to date, there have been no laboratory studies focusing on heterogeneous reactions between DHAA and OH radicals.

Tropospheric temperature varies notably with the change of seasons. Some studies have found that temperature can affect the reactions between different organic compounds and OH radicals.[50,51] For this reason, it is necessary to investigate the effect of temperature on the DHAA–OH reaction for evaluation of the atmospheric lifetime of DHAA. Relative humidity (RH) is variable from 20% to 90% in most areas of the world, which may influence the reaction between organics and OH.[52] Therefore, to study the RH effect on DHAA degradation kinetics by OH, is also necessary to understand the atmospheric behavior of DHAA. Furthermore, in the real atmosphere, organic compounds will mix with other particulate components during transport, which can alter their reactivity toward oxidants. For instance, the heterogeneous reactivity of benzo[*a*]pyrene (BaP) toward O_3 was reduced substantially by a thin (4–8 nm), solid eicosane coating and entirely suppressed by thick (10–80 nm) solid eicosane coatings;[53] the uptake coefficient of N_2O_5 on mixtures of humic acid and $(NH_4)_2SO_4$ decreased by more than a factor of two compared with that of single-component $(NH_4)_2SO_4$.[54] During biomass burning, a number of air pollutants will be generated, with soot being one of the most significant.[55] Furthermore, $(NH_4)_2SO_4$ also constitutes a significant fraction of the total atmospheric particulate mass.[56] It has been found that soot particles can be internally mixed with sulfate.[57,58] These particulate components are likely to mix with DHAA in the ambient atmosphere, thus must be considered when carrying out DHAA degradation studies.

In this study, we present the measured heterogeneous degradation kinetics of particulate dehydroabietic acid exposed to OH radicals under different environmental conditions. The aim of this work is to obtain experimental degradation kinetic parameters and atmospheric lifetimes of DHAA, and further understand the influence of temperature, relative humidity and mixing states on the degradation kinetics. The results obtained in this study will provide an update for kinetic parameters of DHAA in the atmosphere, and provide important information for possible model investigations, especially for source apportionment studies.

Experimental section

Experimental methods

All the experiments were performed using a flow system, which contains a quartz tube irradiated with UV light for OH generation and a stainless steel reactor for dark reaction. The interior walls of the reactor were coated with Teflon to provide a chemically inert surface. The volume of the reactor was 30 cm^3. A Teflon disc (geometric surface area 3.39 cm^2) was used as the sample holder. The schematic diagram of the experimental set-up used in this study is shown in Fig. S1 (ESI†). For the kinetic studies of pure DHAA, 10.0 ± 0.1 μg of DHAA dry film was placed on the disc, which was generated evenly by gently drying a DHAA/methanol solution with N_2 flow. In the case of reactions for the mixed samples, 10.0 ± 0.1 mg of each sample was placed evenly on the disc. Although the DHAA in this study was presented in film form rather than as suspended particles, previous studies have confirmed the feasibility of this method in investigation of the degradation kinetics of levoglucosan and heterogeneous reactions between O_3 and anthracene or NO_2 and anthracene adsorbed on mineral oxides.[59–61]

The reactions between DHAA and OH were carried out under mixed air flow with a constant OH concentration. The total flow rate was 300 mL min^{-1} with simulated air (80% high purity N_2 and 20% high purity O_2) and bubbled H_2O_2 flow. The RH of the system was controlled by varying the ratio of wet N_2 flow, which was achieved by bubbling nitrogen through H_2O, to dry N_2 flow, and determined using a humidity temperature meter (CENTER-314) at the exit of the reactor. The temperature of the system was controlled by a circulating water bath (CCA-20, Gongyi City YUHUA Instrument Co., Ltd) with uncertainty less than 0.5 °C. The water partial pressure in the system may change when the temperature changes, but RH can be kept constant at different temperatures by adjusting the ratio of wet N_2 flow to dry N_2 flow. As direct irradiation of the samples by UV light was avoided (as shown in Fig. S1, ESI†), any decay of reactants should result from oxidation by OH radicals in the dark.

Reacted samples were ultrasonically extracted using 20.0 ± 0.1 mL methanol, and then filtered using a glass fiber filter that had been previously cleaned by methanol. The eluate was evaporated to near dryness, and subsequently transferred into a 1.5 mL sealed vial, then dried to residue under a gentle nitrogen stream.

The high polarity of DHAA demands a derivatization step prior to GC analysis, and silylation is recognized as the best derivatization method to reduce the polarity.[62] *N*,*O*-Bis-(trimethylsilyl)trifluoroacetamide (BSTFA) plus 1% trimethylchlorosilane (TMCS) was chosen to be the silylation reagent for the derivatization of DHAA. In this study, 50 μL of pyridine and 50 μL of BSTFA plus 1% TMCS were added to the residue from the previous steps, and the silylation reaction was performed at 60 °C for 60 minutes. Finally, 1.0 μL of the silylated product was injected into the GC–MS system.

GC was performed with an Agilent Technology 6890N Network GC System, and MS was carried out with an Agilent Technology 5973 Network system with Mass Selective Detector. The capillary column HP-5MS (30 m, 0.25 mm internal diameter, 0.25 μm film thickness) was installed in the GC, and its output was inserted directly into the ion source of the MS. Each sample was introduced *via* EPC splitless mode injection. The oven temperature was held at 80 °C for 1 min, then programmed to 250 °C at a ramp of 12 °C min^{-1} and held at 250 °C for 2 min. Helium was used as carrier gas at a constant flow rate of 1.0 mL min^{-1}. The temperatures of the injector and transfer line were 250 °C and 280 °C, respectively. For quantification of DHAA, mass detection was performed in selected ion monitoring (SIM) mode. The *m*/*z* at 239 was used as the quantification ion and the *m*/*z* at 357 and 372 were used as the confirmation ions for the trimethyl silylation product of DHAA, respectively. The concentration of DHAA was measured based on an external standard and use of a calibration curve.

OH generation and detection

OH radicals were generated in a quartz tube by UV photolysis of H_2O_2. Two ultraviolet light lamps (18 W, Beijing Lighting Research Institute) which provided UV radiation with a central wavelength around 254 nm were used. The concentration of OH radical was controlled by varying the ratio of pure N_2 and H_2O_2 flow passing through the tube.

Salicylic acid has strong reactivity with OH radicals, and can be used to trap them.[63] In this study, the yields of the products (2,3-dihydroxybenzonic acid and 2,5-dihydroxybenzonic acid) during the reactions between salicylic acid and OH were used to estimate the concentration of near-surface OH radicals. To determine OH concentration, the reactions for salicylic acid oxidation occurred concurrently with DHAA oxidation. Detailed descriptions of the experimental procedures for OH determination are given in the ESI.† This method is usually used for liquid phase OH determination, but has been verified in our previous work as the measured k_2 of levoglucosan toward hydroxyl radical is comparable with literature values.[59] In this study, the OH concentration was adjusted to $2.05 \pm 0.06 \times 10^7$, $2.38 \pm 0.08 \times 10^7$ and $2.99 \pm 0.10 \times 10^7$ molecules cm^{-3} for subsequent experiments. Repeat experiments were carried out seven times for each OH concentration. The relative standard deviations (RSD) of OH concentration were less than 10%.

Mixed sample preparation and characterization

To simulate different mixing states, DHAA was mixed with $(NH_4)_2SO_4$ and soot particles. In this study, the symbol A–B represents A internally mixed with B, and the symbol A/B represents A coated on B. Before being mixed with DHAA, $(NH_4)_2SO_4$ was cleaned by ultrasonication in methanol, followed by drying at room temperature, and soot particles were preheated at 300 °C under N_2 protection for 8 h. DHAA was mixed with the particles *via* an impregnation method. Detailed preparation procedures for the mixed samples are given in the ESI.† Three mixed samples were prepared to simulate different mixing states: DHAA–$(NH_4)_2SO_4$ (DHAA–AS), DHAA/soot, and DHAA–$(NH_4)_2SO_4$/soot (DHAA–AS/soot). To maintain a consistent initial concentration of DHAA, 10.0 μg of DHAA was used for each experiment. All the mixed samples were dried at room temperature and stored at −18 °C in the dark.

The mixing state and particle size of the mixed samples were characterized by a scanning electron microscope (SEM, Hitachi SU8000 with an accelerating voltage of 10 kV) and a transmission electron microscope (TEM, Hitachi H-7500 with an acceleration voltage of 80 kV). The SEM and TEM results are shown in Fig. S2 (ESI†). The measured particle size of the mixed samples varied from 52.1 ± 18.7 to 217.6 ± 95.7 nm (shown in Table S1, ESI†). To understand the surface state of the mixed samples, SEM with X-ray microanalysis (SEM-EDX, Hitachi SU8000 with an accelerating voltage of 30 kV) was also used to semi-quantitatively detect the element composition on the surface of DHAA–AS.

Chemicals

All the chemicals were of chromatographic grade and used without further purification. Methanol was obtained from Fisher Scientific. A standard of dehydroabietic acid was purchased from AccuStandard, Inc. *N*,*O*-Bis-(trimethylsilyl) trifluoroacetamide plus trimethylchlorosilane (BSTFA:TMCS = 99 : 1) and salicylic acid (>99.5%) were purchased from Tokyo Chemical Industry Co., Ltd. Pyridine, $(NH_4)_2SO_4$ and 30% H_2O_2 were purchased from Sinopharm Chemical Reagent Co., Ltd. Printex U powder from Degussa (CAS No.: 1333-86-4) was used as a model soot aerosol in this study. This was produced through incomplete combustion of hydrocarbons in the air.[64,65] Its specific surface area is 97.24 m^2 g^{-1}, measured using nitrogen Brunauer–Emmett–Teller (BET) physisorption (Quantachrome Autosorb-1-C). To better understand the size of soot particles, SEM was used (Hitachi SU8000 with an accelerating voltage of 1.0 kV). Images are shown in Fig. S4 (ESI†). The average sizes of soot particles was measured to be 39.8 ± 10.5 nm. High purity N_2 (99.99%) and O_2 (99.99%) were supplied by Beijing HUAYUAN Gases Inc.

Results and discussion

Kinetic measurements for pure dehydroabietic acid

To evaluate the influence of vaporization and degradation by H_2O_2 on dehydroabietic acid, blank experiments were performed under the same air and H_2O_2 flows as those in the oxidation experiments at different temperatures. The experiments were carried out at 40% RH in the dark. As shown in Fig. S5 (ESI†), the decrease in the amount of pure dehydroabietic

acid was less than 10% at 5 °C and 30 °C over 5 hours purging. The experiments in this study were all carried out in the temperature range between 5 °C and 30 °C. Therefore, the slight decrease of DHAA concentration can be ascribed to evaporation of DHAA during purging by air flow. This DHAA evaporation will not prominently affect the measured reaction rate because of its relatively low content, and this effect has been considered in the kinetics interpretation.

To determine the degradation rate constant of pure DHAA toward OH radicals, pure DHAA was oxidized under three different OH concentrations (near-surface gas phase concentration, similarly hereinafter), which had been estimated previously in degradation experiments of salicylic acid. The OH concentrations used in this study were $2.05 \pm 0.06 \times 10^7$, $2.38 \pm 0.08 \times 10^7$ and $2.99 \pm 0.10 \times 10^7$ molecules cm^{-3}.

The kinetic data were determined by monitoring the loss of DHAA concentration as a function of OH exposure at 25 °C with 40% RH in the dark. Assuming a second-order reaction between OH and DHAA, the loss rate of DHAA can be expressed as follows,

$$-\frac{d[DHAA]}{dt} = k_2[OH][DHAA] \quad (1)$$

where [OH] is the near-surface OH concentration (molecules cm^{-3}), [DHAA] is the concentration of dehydroabietic acid and k_2 is the second-order rate constant for the reactions between DHAA and OH (cm^3 $molecule^{-1}$ s^{-1}). As the experiments were performed under steady state conditions with constant OH concentration, eqn (1) can be integrated from zero to the residence time (t) of reactants:

$$\ln\frac{[DHAA]}{[DHAA]_0} = -k_2[OH]t \quad (2)$$

where $[DHAA]_0$ is the initial concentration of dehydroabietic acid. As DHAA cannot be consumed completely, even under high OH exposure, a plateau is always observed in the degradation curve of DHAA. This phenomenon has been widely observed for other reaction systems.[43,66] This plateau might result from the diffusion limit of OH in the solid phase and the influence of oxidation products remaining on the surface. The fraction of DHAA remaining (at the plateau) decreases with increased OH concentration, which may be a result of more OH radicals diffusing into DHAA at the beginning of the reaction after some oxidation products are further oxidized to small molecules with high vapor pressure, which may cause a vacancy on the surface for OH reaction under higher OH concentrations.

Fig. 2 shows the changes in $[DHAA]/[DHAA]_0$ as a function of OH exposure under different OH concentrations at 40% RH and 25 °C. The lines are the exponential curve fitting results, from which the k_2 can be derived *via* eqn (2). The k_2 values under different OH concentrations are listed in Table 1. In general, for the heterogeneous reaction taking place under ambient pressure and on packed powder samples, both external (gaseous reactants from gas phase to the surface) and internal diffusions (from the surface layer to the underneath layers and into the pores of particles or films) need to be corrected.[67–69] However, as discussed in detail in the ESI,† it is not necessary to do both external and internal diffusion corrections for the following reasons. Firstly, the near-surface but not gas phase OH concentrations were measured with a particle phase reference. Secondly, all the samples are nonporous with smooth surfaces. Finally, previous studies have recognized that reactions between OH and organic compounds are limited on the surface.[71]

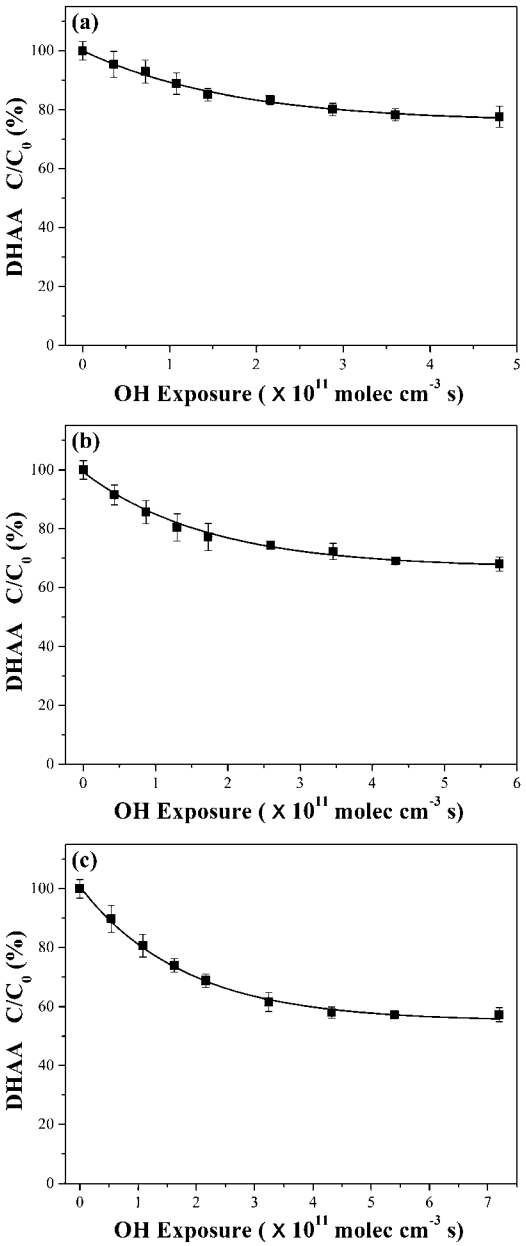

Fig. 2 Representative decays for dehydroabietic acid under different OH concentrations at 25 °C and 40% RH (n = 3, error bars represent 1 standard deviation based on triplicate analyses). (a) [OH] = (2.05 ± 0.06) × 10^7 molecules cm^{-3}; (b) [OH] = (2.38 ± 0.08) × 10^7 molecules cm^{-3}; (c) [OH] = (2.99 ± 0.10) × 10^7 molecules cm^{-3}. Samples were exposed to OH radicals from 0 minutes to 400 minutes (0 min, 30 min, 60 min, 90 min, 120 min, 180 min, 240 min, 300 min and 400 min for each point).

Table 1 Calculated rate constant and atmospheric lifetime of dehydroabietic acid for the reaction between dehydroabietic acid and OH radicals under different atmospheric conditions

Reaction conditions				Second-order rate constant (k_2, cm^3 $molecule^{-1}$ s^{-1})	Atmospheric lifetime[a] (days)
Pure dehydroabietic acid (DHAA)	DHAA–OH reaction under different OH concentrations	OH concentration[b] (molecule cm^{-3})[63,70]	$(2.05 \pm 0.06) \times 10^7$	$(5.69 \pm 0.84) \times 10^{-12}$	—
			$(2.38 \pm 0.08) \times 10^7$	$(5.85 \pm 0.66) \times 10^{-12}$	—
			$(2.99 \pm 0.10) \times 10^7$	$(5.62 \pm 0.51) \times 10^{-12}$	—
			Average	$(5.72 \pm 0.87) \times 10^{-12}$	2.5 ± 0.3
	Literature results for DHAA in the gas phase	AOPWIN estimation[49]		2.73×10^{-11}	0.5
		Quantum chemical calculations[49]		8.9×10^{-12}	1.6
	Temperature effect[c]		5 °C	$(3.90 \pm 0.69) \times 10^{-12}$	3.7 ± 0.6
			15 °C	$(4.80 \pm 0.47) \times 10^{-12}$	3.0 ± 0.3
			20 °C	$(5.10 \pm 0.54) \times 10^{-12}$	2.8 ± 0.3
			25 °C	$(5.62 \pm 0.51) \times 10^{-12}$	2.6 ± 0.2
			30 °C	$(6.16 \pm 0.47) \times 10^{-12}$	2.3 ± 0.2
	RH effect[d]		20%	$(5.44 \pm 0.51) \times 10^{-12}$	2.9 ± 0.3
			40%	$(5.61 \pm 0.32) \times 10^{-12}$	2.8 ± 0.2
			60%	$(5.64 \pm 0.31) \times 10^{-12}$	2.8 ± 0.2
			80%	$(5.32 \pm 0.41) \times 10^{-12}$	2.9 ± 0.2
Mixed samples[e]	DHAA–$(NH_4)_2SO_4$			$(4.58 \pm 0.95) \times 10^{-12}$	3.2 ± 0.5
	DHAA/soot			$(3.30 \pm 0.79) \times 10^{-12}$	4.4 ± 0.8
	$(NH_4)_2SO_4$–DHAA/soot			$(3.52 \pm 0.91) \times 10^{-12}$	4.1 ± 0.8

[a] Assuming the typical concentration for 12 h average value of OH to be 1.6×10^6 molecules cm^{-3}. [b] Experimental condition: RH = 40%, temperature = 25 °C. [c] Experimental condition: [OH] = $(2.99 \pm 0.10) \times 10^7$ molecules cm^{-3}, RH = 40%. [d] Experimental condition: [OH] = $(2.99 \pm 0.10) \times 10^7$ molecules cm^{-3}, temperature = 25 °C. [e] Experimental condition: [OH] = $(2.99 \pm 0.10) \times 10^7$ molecules cm^{-3}, RH = 40%, temperature = 25 °C.

At 25 °C, the k_2 values for DHAA–OH reactions were similar for different OH concentrations (Table 1), with an average of $5.72 \pm 0.87 \times 10^{-12}$ cm^3 $molecule^{-1}$ s^{-1}. This implies that the experimental conditions are controllable and repeatable. Under the same conditions, the measured k_2 for DHAA toward OH in this study is significantly ($P = 3.94 \times 10^{-8}$ at 0.95 confidence level in one-way ANOVA analysis) smaller than that of levoglucosan ($9.17 \pm 1.16 \times 10^{-12}$ cm^3 $molecule^{-1}$ s^{-1} at 25 °C and 40% RH).[59] The difference between the measured k_2 of DHAA and levoglucosan highlights the role of structure in reactivity of organics to OH. Using the Atmospheric Oxidation Program for Microsoft Windows (AOPWIN) model, which is based on structure–activity relationship (SAR) methods developed by Atkinson and coworkers,[51,72] the k_2 of DHAA in the gas phase was estimated to be 2.73×10^{-11} cm^3 $molecule^{-1}$ s^{-1}, whereas it was calculated to be 8.9×10^{-12} cm^3 $molecule^{-1}$ s^{-1} using quantum chemical calculations.[49] The average rate constant for the heterogeneous reaction between DHAA and OH radicals measured in this study is lower than the values calculated by both the quantum chemical program and the AOPWIN model. For levoglucosan, although the measured k_2 from our previous study shows good agreement with the chamber experiment result ($(1.1 \pm 0.5) \times 10^{-11}$ cm^3 $molecule^{-1}$ s^{-1}),[36] it is below the result obtained by SAR calculation (5.28×10^{-11} cm^3 $molecule^{-1}$ s^{-1})[73] and much higher than that obtained using quantum chemical calculations (2.21×10^{-13} cm^3 $molecule^{-1}$ s^{-1}).[74] A recent study reported that the AOPWIN model overestimates the second-order rate constant of the reaction of organic aerosol with OH in the particle phase,[75] which is consistent with results of the present study. The results obtained from this study also imply that the lifetime of organics might be underestimated using gas-phase kinetic data (SAR-based k_2); however, this requires confirmation by field measurements in remote regions. If these compounds can be observed in remote areas where the sources of the compound does not exist, then this would imply that its lifetime is long enough for transfer to such areas.

Effect of temperature

To investigate the effect of different temperatures, the temperature of the system was regulated at 5 °C, 15 °C, 20 °C, 25 °C and 30 °C under a constant RH of 40%. Temperatures under 5 °C might cause some water vapor condensation on the surface of the sample holder, with the potential for errors in measurements of DHAA concentration. Thus, experiments at temperature lower than 5 °C were not performed in this study. The concentration of OH radical was adjusted to $2.99 \pm 0.10 \times 10^7$ molecules cm^{-3} and all the experiments were conducted in the dark.

The kinetic data were determined by monitoring loss of DHAA concentration as a function of OH exposure. The changes in $[DHAA]/[DHAA]_0$ as a function of OH exposure under different temperatures at 40% RH are shown in Fig. 3. The lines are the exponential curve fitting results, from which the k_2 can be derived *via* eqn (2). The k_2 values calculated at different temperatures are listed in Table 1. From these results, degradation of dehydroabietic acid was significantly influenced by temperature. The k_2 increased from $3.90 \pm 0.69 \times 10^{-12}$ cm^3 $molecule^{-1}$ s^{-1} at 5 °C to $6.16 \pm 0.47 \times 10^{-12}$ cm^3 $molecule^{-1}$ s^{-1} at 30 °C.

Fig. 4 shows the Arrhenius plot of the measured rate constants for the reaction between DHAA and OH, for which the Arrhenius expression is $k_2 = (8.9 \pm 1.9) \times 10^{-10} \exp[-(1508.2 \pm 64.2)/T]$ in units of cm^3 $molecule^{-1}$ s^{-1}. A positive temperature dependence

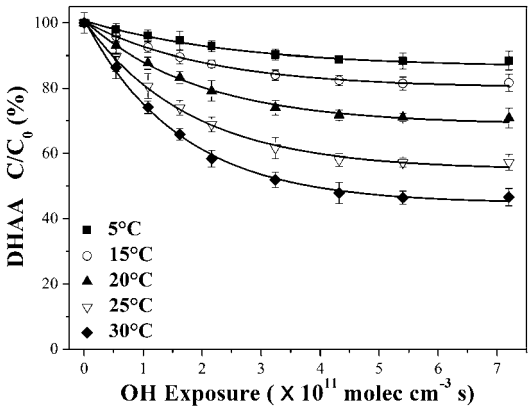

Fig. 3 Representative decays for dehydroabietic acid at different temperature with a constant relative humidity of 40% as a function of OH exposure (n = 3, error bars represent 1 standard deviation based on triplicate analyses).

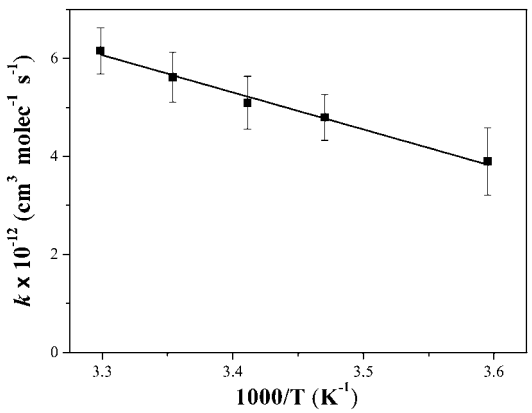

Fig. 4 Measured rate constants for the reaction between dehydroabietic acid and OH radical as a function of temperature.

was observed for this reaction, with the overall activation energy calculated to be 12.5 ± 0.5 kJ mol^{-1}. Some studies have found that temperature can either positively or negatively affect the reactions between different organic compounds and OH radicals.[50,51] High temperature may affect gas/particle partitioning process,[76] thus leading to more gas phase DHAA in the reactor. The phase state of particles has been found to play an important role in heterogeneous reactions.[77] Transformation from the solid phase to semi-solid or liquid phase will promote heterogeneous reaction, because particle-phase diffusion becomes faster as a result of the lower viscosity of organic matter. However, the melting point of DHAA is 447–449 K, which is much higher than the highest temperature (303 K) in this study, so the narrow temperature range should have no influence on the phase state of the DHAA film. The positive temperature dependence of the rate constant means that there is an activation energy for the formation of the transition state and that the reactivity is promoted by higher temperatures. In a previous study, Bai *et al.* calculated the activation energies for DHAA–OH reaction with a large range between 0.97 and 18.08 kJ mol^{-1} for different elementary reactions with an average of 7.6 ± 5.1 kJ mol^{-1}.[49] In this study, overall activation energy was measured. Although it is difficult to directly compare these activation energies, their tendencies are consistent, namely, higher temperatures promote this reaction. Similarly, for levoglucosan–OH reactions the overall activation energy was measured to be 16.0 ± 2.2 kJ mol^{-1},[59] also implying a promotion effect by high temperature.[37] This is analogous to the observed variation in DHAA and levoglucosan degradation with environmental temperature. DHAA and levoglucosan are two of the main biomass burning tracers, as degradation of both shows positive temperature dependence. More attention should be paid to OH oxidation of biomass burning tracers when source apportionment is carried out in different seasons.

Effect of relative humidity

To investigate the effect of different levels of RH on the degradation kinetics of DHAA by OH, the RH of the system was adjusted to 20%, 40%, 60% and 80% under a constant temperature of 25 °C. The concentration of OH radical was adjusted to 2.99 ± 0.10 × 10^7 molecules cm^{-3}. The changes in [DHAA]/[DHAA]$_0$ as a function of OH exposure under different RH at 25 °C are shown in Fig. 5. The k_2 values for DHAA–OH reactions calculated by eqn (2) are listed in Table 1. Results indicate that DHAA was rarely influenced by RH when temperature was fixed. It has been found that RH can positively or negatively influence reactions between OH and the organic particles. Some researchers have observed that increased RH will lower the viscosity of the amorphous aerosol particles and subsequently enhance OH uptake because particle-phase diffusion is feasible,[78–80] whereas other results show that the OH uptake was suppressed at higher RH because of competitive co-adsorption of water, which will take up the reactive sites.[52] Based on our previous study, degradation of levoglucosan by OH was influenced significantly by RH because of different layers of water cover on the surface of levoglucosan under different relative humidities. In this study, as the solubility of DHAA in water is rather low, variation of RH will not change the water content covering the surface of DHAA, thus has little influence on the degradation kinetics of DHAA when exposed to OH.

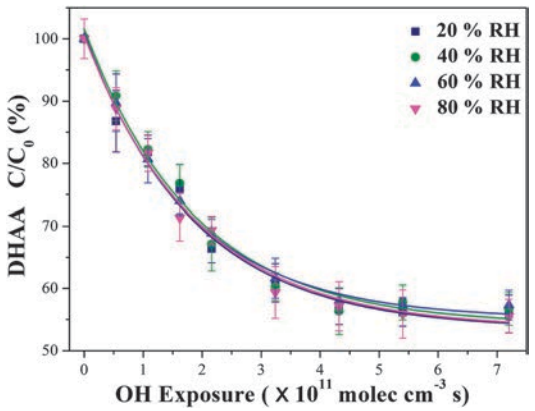

Fig. 5 Representative decays for dehydroabietic acid at different relative humidity with a constant temperature of 25 °C as a function of OH exposure. (n = 3, error bars represent 1 standard deviation based on triplicate analyses).

Effect of different mixing states

To simulate different mixing states possibly present in the atmosphere, DHAA was mixed with $(NH_4)_2SO_4$, soot particles, and both $(NH_4)_2SO_4$ and soot. $(NH_4)_2SO_4$ and soot were chosen to mix with DHAA and simulate the ambient process for the following reasons. Firstly, sulfate contributes 30% of total atmospheric particles, which may mix with other species in the atmosphere. Secondly, as DHAA is mainly emitted from biomass combustion, it may mix with soot particles, thus mixtures of DHAA and soot are possible in the real atmosphere. Moreover, in the troposphere, heterogeneous reactions of trace gases, including SO_2 and NH_3, can take place on the soot surface. This results in internally mixed particles, which have been observed in field measurements.[57,58] Therefore, similar to other organic components, which have been found to mix with $(NH_4)_2SO_4$ and soot,[81–83] DHAA mixed with both soot and $(NH_4)_2SO_4$ may exist in the ambient air. As DHAA represents a series of compounds emitted from conifer wood combustion, which can be detected in relatively large quantities,[5] the three mixing states represent well the real situation of DHAA.

The reactions between DHAA mixed samples and OH radicals were performed in the dark at 25 °C and 40% RH. The concentration of OH radical was $2.99 \pm 0.10 \times 10^7$ molecules cm^{-3}. Fig. 6 shows the degradation curves for DHAA mixed samples, and the calculated k_2 values are listed in Table 1. Through one-way analysis of variance (ANOVA), it was confirmed that the rate coefficients of the reactions between OH and DHAA, DHAA–$(NH_4)_2SO_4$ and DHAA/soot do have significant differences, with $P < 0.05$ (0.0399) at 0.95 confidence level. Therefore, degradation of DHAA by OH radical was significantly influenced by the mixing states. When mixed with $(NH_4)_2SO_4$ (corresponding to DHAA–AS), the rate constant of the degradation of DHAA by OH radical decreased to $4.58 \pm 0.9 \times 10^{-12}$ cm^3 $molecule^{-1}$ s^{-1} compared with pure DHAA. Based on semi-quantitative analysis carried out by SEM-EDX, the carbon content on the surface of DHAA–AS was determined to be 7.44% (by wt). The carbon content on the surface of DHAA–AS is higher than that of pure $(NH_4)_2SO_4$, which means there is some DHAA on the surface of $(NH_4)_2SO_4$; but lower than hypothetical condition that DHAA were all on the surface of $(NH_4)_2SO_4$. This indicates that some DHAA may be encased by $(NH_4)_2SO_4$. Therefore, internally mixed $(NH_4)_2SO_4$ and DHAA was formed. The reduction of the rate constant might be related to the internally mixed $(NH_4)_2SO_4$ and DHAA, in which the $(NH_4)_2SO_4$ on the surface of the mixed sample may slightly inhibit diffusion of OH on the surface. When mixed with soot (corresponding to DHAA/soot), the degradation rate of DHAA by OH decreased to $3.30 \pm 0.79 \times 10^{-12}$ cm^3 $molecule^{-1}$ s^{-1}, showing a more obvious inhibition effect compared with $(NH_4)_2SO_4$. As the surface area of soot is relatively high (97.24 m^2 g^{-1}), it is reasonable to infer that DHAA may enter the inner channels of soot, thus impeding contact between DHAA and OH radicals. On the other hand, soot is also reactive toward OH,[84] and the completive reaction of the soot toward OH will reduce reaction between DHAA and OH because of the decrease in effective surface concentration of OH. When mixed with both soot and $(NH_4)_2SO_4$ (corresponding to DHAA–AS/soot), as shown in Table 1, the degradation rate of DHAA by OH was similar to that of the mixed sample DHAA/soot. This implies that reactivity of the soot on the surface toward OH might be the main reason for reduction of reactivity of DHAA in this complicated mixing state.

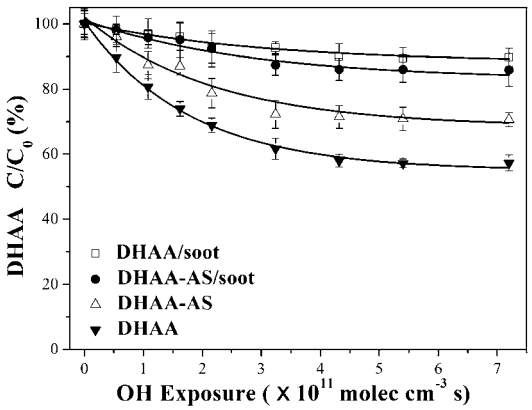

Fig. 6 Representative DHAA decays under different mixing states as a function of OH exposure at 25 °C and 40% RH (n = 3, error bars represent 1 standard deviation based on triplicate analyses).

Conclusions and atmospheric implications

In this study, the degradation behaviors of DHAA toward OH radicals were measured using a flow reactor under different conditions to understand the atmospheric stability of DHAA. When exposed to OH radicals, conspicuous degradation of DHAA was observed. Temperature and the mixing state also play important roles in the degradation rate. The second-order rate constant (k_2) for degradation of pure DHAA in the particulate phase by OH was measured to be $5.72 \pm 0.87 \times 10^{-12}$ cm^3 $molecule^{-1}$ s^{-1} at 25 °C and 40% RH. This value is lower than those estimated in the gas phase. At 40% RH, the k_2 of pure DHAA increased with increasing temperature, as expressed in the Arrhenius equation $k_2 = (8.9 \pm 1.9) \times 10^{-10} \exp[(-1508.2 \pm 64.2)/T]$, while RH had no significant impact at 25 °C. Mixtures of DHAA with soot (DHAA/soot) showed more prominent inhibition of the degradation rate than mixtures with $(NH_4)_2SO_4$. When mixed with both soot and $(NH_4)_2SO_4$, no additional inhibition by $(NH_4)_2SO_4$ was observed compared with DHAA/soot.

OH, NO_3, Cl radicals and O_3 are the main effective oxidants in the atmosphere, of which OH is considered to be the most dominant during the daytime for organics.[72,85] Therefore, the rate coefficients obtained in this study can be used to calculate the atmospheric lifetime of DHAA exposed to OH radicals. The atmospheric lifetime of DHAA (τ) was calculated according to the following equation:

$$\tau = \frac{1}{k_2[\mathrm{OH}]} \quad (3)$$

Assuming a 12 h average OH concentration to be 1.6×10^6 molecules cm^{-3} during daytime (25 °C and 101 kPa),[86,87] the atmospheric lifetime of pure DHAA in the particle phase was calculated to be 2.5 ± 0.3 days. This value is prominently larger than the calculated lifetimes based on the rate constants in the gas phase, which suggests that modeling or quantum chemical calculations underestimate the lifetimes of organics in particulate matter. Under different environmental conditions, the lifetimes varied from 2.3 ± 0.2 to 4.4 ± 0.8 days, as shown in Table 1, indicating that temperature and mixing states have remarkable impacts on the degradation kinetics and lifetime of DHAA. In particular, soot particles may have a prominent effect on the degradation kinetics. Therefore, the degradation kinetics determined for pure DHAA should be the upper limit of that in the real troposphere. As DHAA is mainly produced during combustion, the kinetics data for DHAA on soot should be more realistic than those for pure DHAA.

It should be pointed out that the longest lifetime of DHAA measured in this study is still shorter than the residence time of aerosols in the troposphere. This means that the concentration of DHAA measured in field measurements for the purpose of source apportionment might have been underestimated in the past, thus introducing a negative error in source apportionment. For other sources, such as engine exhaust, Lambe *et al.* also pointed out that neglecting degradation of engine exhaust tracers (*n*-alkanes, hopanes and steranes) by OH may lead to a significant error in source apportionment.[41] As all these tracers show high reactivity towards OH radicals, understanding of the fate of these tracers in the atmosphere should be updated to ensure more effective results in source apportionment.

Acknowledgements

This research was supported by the National Natural Science Foundation of China (21190054, 51221892) and the Strategic Priority Research Program of the Chinese Academy of Sciences (XDB05010300, XDB05040100).

Notes and references

1 D. A. Knopf, S. M. Forrester and J. H. Slade, *Phys. Chem. Chem. Phys.*, 2011, **13**, 21050–21062.
2 M. Kanakidou, J. H. Seinfeld, S. N. Pandis, I. Barnes, F. J. Dentener, M. C. Facchini, R. Van Dingenen, B. Ervens, A. Nenes, C. J. Nielsen, E. Swietlicki, J. P. Putaud, Y. Balkanski, S. Fuzzi, J. Horth, G. K. Moortgat, R. Winterhalter, C. E. L. Myhre, K. Tsigaridis, E. Vignati, E. G. Stephanou and J. Wilson, *Atmos. Chem. Phys.*, 2005, **5**, 1053–1123.
3 F. Duan, K. He, Y. Ma, Y. Jia, F. Yang, Y. Lei, S. Tanaka and T. Okuta, *Chemosphere*, 2005, **60**, 355–364.
4 J. Aldabe, D. Elustondo, C. Santamaría, E. Lasheras, M. Pandolfi, A. Alastuey, X. Querol and J. M. Santamaría, *Atmos. Res.*, 2011, **102**, 191–205.
5 R. M. Qadir, G. Abbaszade, J. Schnelle-Kreis, J. C. Chow and R. Zimmermann, *Environ. Pollut.*, 2013, **175**, 158–167.
6 J. C. Chow and J. G. Watson, *Energy Fuels*, 2002, **16**, 222–260.
7 K. Saarnio, K. Teinila, M. Aurela, H. Timonen and R. Hillamo, *Anal. Bioanal. Chem.*, 2010, **398**, 2253–2264.
8 R. M. Healy, S. Hellebust, I. Kourtchev, A. Allanic, I. P. O'Connor, J. M. Bell, D. A. Healy, J. R. Sodeau and J. C. Wenger, *Atmos. Chem. Phys.*, 2010, **10**, 9593–9613.
9 D. Hu, Q. Bian, A. K. H. Lau and J. Z. Yu, *J. Geophys. Res.*, 2010, **115**, D16204.
10 V. A. Lanz, M. R. Alfarra, U. Baltensperger, B. Buchmann, C. Hueglin and A. S. H. Prevot, *Atmos. Chem. Phys.*, 2007, **7**, 1503–1522.
11 E. Stone, J. Schauer, T. A. Quraishi and A. Mahmood, *Atmos. Environ.*, 2010, **44**, 1062–1070.
12 E. A. Stone, D. C. Snyder, R. J. Sheesley, A. P. Sullivan, R. J. Weber and J. J. Schauer, *Atmos. Chem. Phys.*, 2008, **8**, 1249–1259.
13 Y. Chen, M. Zheng, E. S. Edgerton, L. Ke, G. Sheng and J. Fu, *J. Geophys. Res.*, 2012, **117**, D08304.
14 L. Lin, M. L. Lee and D. J. Eatough, *J. Air Waste Manage. Assoc.*, 2010, **60**, 3–25.
15 E. Vermote, E. Ellicott, O. Dubovik, T. Lapyonok, M. Chin, L. Giglio and G. J. Roberts, *J. Geophys. Res.*, 2009, **114**, D18205.
16 M. Fang, M. Zheng, F. Wang, K. L. To, A. B. Jaafar and S. L. Tong, *Atmos. Environ.*, 1999, **33**, 783–795.
17 K. Kawamura, Y. Izawa, M. Mochida and T. Shiraiwa, *Geochim. Cosmochim. Acta*, 2012, **99**, 317–329.
18 J. S. Levine, W. R. Cofer, D. R. Cahoon and E. L. Winstead, *Environ. Sci. Technol.*, 1995, **29**, A120–A125.
19 B. R. T. Simoneit, *Appl. Geochem.*, 2002, **17**, 129–162.
20 P. M. Fine, G. R. Cass and B. R. T. Simoneit, *Environ. Sci. Technol.*, 2002, **36**, 1442–1451.
21 W. F. Rogge, L. M. Hildemann, M. A. Mazurek, G. R. Cass and B. R. T. Simoneit, *Environ. Sci. Technol.*, 1998, **32**, 13–22.
22 L. J. Standley and B. R. T. Simoneit, *J. Atmos. Chem.*, 1994, **18**, 1–15.
23 C. Gonçalves, C. Alves, A. P. Fernandes, C. Monteiro, L. Tarelho, M. Evtyugina and C. Pio, *Atmos. Environ.*, 2011, **45**, 4533–4545.
24 A. Vicente, C. Alves, A. I. Calvo, A. P. Fernandes, T. Nunes, C. Monteiro, S. M. Almeida and C. Pio, *Atmos. Environ.*, 2013, **71**, 295–303.
25 B. R. T. Simoneit and V. O. Elias, *Mar. Pollut. Bull.*, 2001, **42**, 805–810.
26 M. Xie, G. Wang, S. Hu, S. Gao, Q. Han, Y. Xu and J. Feng, *Sci. Total Environ.*, 2010, **408**, 5452–5460.
27 Y. Zhang, D. Obrist, B. Zielinska and A. Gertler, *Atmos. Environ.*, 2013, **72**, 27–35.
28 A. Caseiro and C. Oliveira, *J. Environ. Monit.*, 2012, **14**, 2261–2269.
29 M. Bergauff, T. Ward, C. Noonan and C. P. Palmer, *Atmos. Environ.*, 2009, **43**, 2938–2943.

30 Z. Krivacsy, M. Blazso and D. Shooter, *Environ. Pollut.*, 2006, **139**, 195–205.
31 A. Leithead, S.-M. Li, R. Hoff, Y. Cheng and J. Brook, *Atmos. Environ.*, 2006, **40**, 2721–2734.
32 M. Mochida, K. Kawamura, P. Fu and T. Takemura, *Atmos. Environ.*, 2010, **44**, 3511–3518.
33 M. C. Pietrogrande, G. Abbaszade, J. Schnelle-Kreis, D. Bacco, M. Mercuriali and R. Zimmermann, *Environ. Pollut.*, 2011, **159**, 1861–1868.
34 A. L. Robinson, R. Subramanian, N. M. Donahue, A. Bernardo-Bricker and W. F. Rogge, *Environ. Sci. Technol.*, 2006, **40**, 7811–7819.
35 J. J. Schauer, W. F. Rogge, L. M. Hildemann, M. A. Mazurek, G. R. Cass and B. R. T. Simoneit, *Atmos. Environ.*, 1996, **30**, 3837–3855.
36 C. J. Hennigan, A. P. Sullivan, J. L. Collett and A. L. Robinson, *Geophys. Res. Lett.*, 2010, **37**, L09806.
37 D. Hoffmann, A. Tilgner, Y. Iinuma and H. Herrmann, *Environ. Sci. Technol.*, 2010, **44**, 694–699.
38 S. H. Kessler, J. D. Smith, D. L. Che, D. R. Worsnop, K. R. Wilson and J. H. Kroll, *Environ. Sci. Technol.*, 2010, **44**, 7005–7010.
39 M. Shiraiwa, U. Poschl and D. A. Knopf, *Environ. Sci. Technol.*, 2012, **46**, 6630–6636.
40 J. H. Slade and D. A. Knopf, *Phys. Chem. Chem. Phys.*, 2013, **15**, 5898–5915.
41 A. T. Lambe, M. A. Miracolo, C. J. Hennigan, A. L. Robinson and N. M. Donahue, *Environ. Sci. Technol.*, 2009, **43**, 8794–8800.
42 E. A. Weitkamp, A. T. Lambe, N. M. Donahue and A. L. Robinson, *Environ. Sci. Technol.*, 2008, **42**, 7950–7956.
43 C. Coeur-Tourneur, A. Cassez and J. C. Wenger, *J. Phys. Chem. A*, 2010, **114**, 11645–11650.
44 Q. Zhang, R. Gao, F. Xu, Q. Zhou, G. Jiang, T. Wang, J. Chen, J. Hu, W. Jiang and W. Wang, *Environ. Sci. Technol.*, 2014, **48**, 5051–5057.
45 Y. Sun, Q. Zhang, J. Hu, J. Chen and W. Wang, *Chemosphere*, 2015, **119**, 626–633.
46 J. Dang, X. Shi, Q. Zhang, J. Hu, J. Chen and W. Wang, *Sci. Total Environ.*, 2014, **490**, 639–646.
47 N. S. Corin, P. H. Backlund and M. A. M. Kulovaara, *Environ. Sci. Technol.*, 2000, **34**, 2231–2236.
48 V. J. Martin, Z. Yu and W. W. Mohn, *Arch. Microbiol.*, 1999, **172**, 131–138.
49 J. Bai, X. Sun, C. Zhang, Y. Zhao and C. Gong, *Chemosphere*, 2013, **92**, 933–940.
50 J. G. Calvert, A. Mellouki, J. Orlando, M. Pilling and T. Wallington, *Mechanisms of atmospheric oxidation of the oxygenates*, Oxford University Press, 2011.
51 R. Atkinson and J. Arey, *Chem. Rev.*, 2003, **103**, 4605–4638.
52 J. H. Slade and D. A. Knopf, *Geophys. Res. Lett.*, 2014, **41**, 5297–5306.
53 S. Zhou, A. K. Y. Lee, R. D. McWhinney and J. P. D. Abbatt, *J. Phys. Chem. A*, 2012, **116**, 7050–7056.
54 C. L. Badger, P. T. Griffiths, I. George, J. P. Abbatt and R. A. Cox, *J. Phys. Chem. A*, 2006, **110**, 6986–6994.
55 J. A. Kozinski and R. Saade, *Fuel*, 1998, **77**, 225–237.
56 D. D. Weis and G. E. Ewing, *J. Geophys. Res.*, 1999, **104**, 21275–21285.
57 W. Li, L. Shao, R. Shen, S. Yang, Z. Wang and U. Tang, *J. Air Waste Manage. Assoc.*, 2011, **61**, 1166–1173.
58 W. Li, L. Shao, Z. Shi, J. Chen, L. Yang, Q. Yuan, C. Yan, X. Zhang, Y. Wang, J. Sun, Y. Zhang, X. Shen, Z. Wang and W. Wang, *J. Geophys. Res.*, 2014, **119**, 1044–1059.
59 C. Lai, Y. Liu, J. Ma, Q. Ma and H. He, *Atmos. Environ.*, 2014, **91**, 32–39.
60 J. Ma, Y. Liu and H. He, *Atmos. Environ.*, 2010, **44**, 4446–4453.
61 J. Ma, Y. Liu and H. He, *Atmos. Environ.*, 2011, **45**, 917–924.
62 M. C. Pietrogrande, D. Bacco and M. Mercuriali, *Anal. Bioanal. Chem.*, 2010, **396**, 877–885.
63 C. C. Chiueh, G. Krishna, P. Tulsi, T. Obata, K. Lang, S.-J. Huang and D. L. Murphy, *Free Radical Biol. Med.*, 1992, **13**, 581–583.
64 J. P. A. Neeft, M. Makkee and J. A. Moulijn, *Fuel*, 1998, **77**, 111–119.
65 K. Villani, W. Vermandel, K. Smets, D. Liang, G. Van Tendeloo and J. A. Martens, *Environ. Sci. Technol.*, 2006, **40**, 2727–2733.
66 T. Berndt and S. Richters, *Atmos. Environ.*, 2012, **47**, 316–322.
67 L. F. Keyser, S. B. Moore and M. T. Leu, *J. Phys. Chem.*, 1991, **95**, 5496–5502.
68 G. M. Underwood, P. Li, H. Al-Abadleh and V. H. Grassian, *J. Phys. Chem. A*, 2001, **105**, 6609–6620.
69 J. F. Widmann and E. J. Davis, *J. Aerosol Sci.*, 1997, **28**, 87–106.
70 B. Yao, T. Zhu and W. Lin, *Environ. Chem.*, 2006, **25**, 772–775.
71 I. J. George and J. P. Abbatt, *Nat. Chem.*, 2010, **2**, 713–722.
72 R. Atkinson, *Chem. Rev.*, 1985, **85**, 69–201.
73 W. M. Meylan and P. H. Howard, *Chemosphere*, 1993, **26**, 2293–2299.
74 J. Bai, X. Sun, C. Zhang, Y. Xu and C. Qi, *Chemosphere*, 2013, **93**, 2004–2010.
75 Y. Liu, J. Liggio, T. Harner, L. Jantunen, M. Shoeib and S. M. Li, *Environ. Sci. Technol.*, 2014, **48**, 1041–1048.
76 X. Ding, X.-M. Wang and M. Zheng, *Atmos. Environ.*, 2011, **45**, 1303–1311.
77 H. Saathoff, K. H. Naumann, O. Möhler, Å. M. Jonsson, M. Hallquist, A. Kiendler-Scharr, T. F. Mentel, R. Tillmann and U. Schurath, *Atmos. Chem. Phys.*, 2009, **9**, 1551–1577.
78 L. P. Chan and C. K. Chan, *Aerosol Sci. Technol.*, 2012, **46**, 236–247.
79 M. Kuwata and S. T. Martin, *Proc. Natl. Acad. Sci. U. S. A.*, 2012, **109**, 17354–17359.
80 Y. Liu, L. Huang, S. M. Li, T. Harner and J. Liggio, *Atmos. Chem. Phys.*, 2014, **14**, 12195–12207.
81 K. Adachi and P. R. Buseck, *Atmos. Chem. Phys.*, 2008, **8**, 6469–6481.
82 S. D. Brooks, M. E. Wise, M. Cushing and M. A. Tolbert, *Geophys. Res. Lett.*, 2002, **29**, 23-1–23-4.

83 M. Schnaiter, H. Horvath, O. Möhler, K. H. Naumann, H. Saathoff and O. W. Schöck, *J. Aerosol Sci.*, 2003, **34**, 1421–1444.
84 C. P. Fenimore and G. W. Jones, *J. Phys. Chem.*, 1967, **71**, 593–597.
85 R. Atkinson, in *Air Pollution, the Automobile, and Public Health*, ed. D. Kennedy and R. Bates, National Academy Press, Washington, D. C., 1988, pp. 99–132.
86 R. Prinn, D. Cunnold, P. Simmonds, F. Alyea, R. Boldi, A. Crawford, P. Fraser, D. Gutzler, D. Hartley and R. Rosen, *J. Geophys. Res.*, 1992, **97**, 2445–2461.
87 R. Prinn, D. Cunnold, R. Rasmussen, P. Simmonds, F. Alyea, A. Crawford, P. Fraser and R. Rosen, *Science*, 1987, **238**, 945–950.

